Stiffness Percolation in Stochastically Fragmented Continua

Anirban Pal and Catalin R. Picu*
Department of Mechanical, Aerospace, and Nuclear Engineering, Rensselaer Polytechnic Institute, Troy, New York 12180, USA
(Received 25 April 2017; published 25 August 2017)

We study the mechanical behavior of three-dimensional, randomly microcracked continua for crack densities up to and above the transport percolation threshold. We show the existence of a fully fragmented material state in which stiffness is preserved due to topological interlocking of fragments. In this regime, the mechanical behavior is controlled by the contacts between fragments and becomes nonlinear. The upper limit of crack densities for which this behavior is observed, the stiffness percolation threshold, is identified. The variation of the effective material stiffness for crack densities ranging from 0 to the stiffness percolation threshold is reported.

DOI: 10.1103/PhysRevLett.119.085502

Rigidity percolation has been studied extensively in random networks [1–3], granular media, and foams [4,5]. It had been shown early [6] that rigidity percolation is not necessarily identical to transport percolation. In random fiber networks, the transition is continuous in both the bulk and shear moduli [1,2,7], while the jamming transition exhibits continuous and discontinuous behaviors for shear and bulk moduli, respectively [4,8–10]. The stiffness percolation threshold in random networks of fibers depends on the type of interactions. If filaments store energy in both the axial and bending deformation modes, the network acquires rigidity at the transport percolation threshold, while when the bending mode is disabled, stiffness percolation happens at higher densities than transport percolation [11].

Continua with large density of microcracks are expected to share some of these features. Although the effective properties of diffusively microcracked continua have been evaluated for relatively small densities of microcracks, e.g., [12], the behavior as the crack density approaches the fully fragmented state has been poorly investigated to date [13]. It is generally believed that when the crack density is so large that the sample becomes fragmented, i.e., divided in multiple components by contiguous cracks, the material has zero tensile stiffness [13]. This has been recently shown to be incorrect in two dimensions (2D), with the crack density at which stiffness vanishes, f_{c_E}, being larger than that corresponding to transport percolation, f_{c_T} [14]. In 2D the crack density at which fragmentation takes place, f_F, is identical to the transport percolation threshold.

Here we identify the transport percolation, fragmentation, and stiffness percolation thresholds in the three-dimensional case and show the existence of a regime in which the material is fully fragmented but preserves stiffness. The stiffness of the body is nonzero due to topological interlocking of fragments. This state of matter is distinct from the granular state due to the presence of tensile stiffness and ordered arrangement of fragments. The material behavior becomes nonlinear, even though the constitutive behavior of the fragments is linear, due to the important contribution of contacts to the overall mechanics. Emergence of nonlinear behavior close to critical points is observed in other systems and phenomena [15]. The notion that a material can be both hard towards indentation while soft in bending is not intuitive, and can be realized using highly microcracked continua, where compliance in tension and bending is a manifestation of fragment interlocking [14], while the response to indentation is provided by individual fragments.

Recently, artificial mechanical metamaterials have been studied due to their novel properties stemming from careful design of their substructures [16,17]. Interlocking was recently used to produce such a class of metamaterials whose behavior is controlled by the contacts between components and depends less on the constitutive behavior of individual components. These studies considered assemblies of identical and periodically arranged interlocking objects held together either by their shape or by a confining pressure [18–21]. Such assemblies are damage tolerant, as any load-induced crack is trapped at the interfaces between components [22,23]. Porous superlattice has been created by the topological interlocking of self-assembled nanoscale octapods [24]. Interlocking of asperities across an interface with otherwise poor adhesion may lead to increased opening strength and is known to increase the mode II fracture toughness when the interface is loaded in shear [25]. The present study shows that interlocking occurs naturally in materials with stochastic cracking patterns and the effect can be obtained without the need to artificially assemble identical components. This is believed to be the case in naturally occurring itacolumite, which is a sandstone [26]. This rock is composed from roughly equiaxed grains that form clusters that are separated by gaps of micron-scale thickness. The gaps allow the relative motion of the clusters that conveys flexibility to the rock on the macroscopic scale. However, the rock has nonzero tensile

stiffness due to cluster interlocking. A movie demonstrating this behavior is presented in [14]. Such observations motivated efforts to develop flexible ceramics [27]. These are obtained by subjecting regular ceramic materials to thermal shock, which leads to intergranular cracking. The resulting microstructure mimics that of itacolumite and is similar to the structures considered in this study. Our results indicate the range of parameters in which a continuum becomes flexible, while preserving finite stiffness in both tension and compression.

We start with a face-centered cubic (fcc) lattice of N^3 unit cells defined within a large cubic domain, D, of edge size L, and construct a Voronoi tessellation using the lattice sites as seeds, which leads to a packed tiling of identical rhombic dodecahedra. The nearest-neighbor bonds of the fcc lattice are normal to, and are bisected by, the bounding faces of the corresponding Voronoi cells. Cracks are introduced randomly on the faces of the tiling. The crack density is defined by the fraction f of cracked faces; at $f = 1$ all Voronoi faces are cracked. The stochasticity of the cracked structure emerges from the randomness of the face-selection process, as the cell shapes and positions are regular. This contrasts with the previous 2D study of the equivalent problem [14], where stochasticity originates both from the variability of the Voronoi cell shapes associated with the random distribution of seeds in 2D, as well as from the crack face-selection procedure. In polycrystals with weak grain boundaries microcracking takes place stochastically if the distribution of boundary strengths is broad and the crack density is relatively low. Some degree of correlation may exist in the case of narrow strength distributions and/or higher crack densities when the nucleation process is controlled predominantly by the local field fluctuations induced by the microcracks themselves.

The transport percolation threshold, f_{c_T}, is defined as the crack density at which a crack path connecting opposite faces of the cubic domain, $\mathcal{D}$, first forms. Here a crack path is defined as a contiguous set of crack faces, each face meeting its neighbors at its edges. Hence, this threshold is equivalent to the site percolation threshold on a lattice formed by the Voronoi face centers, which turns out to be an edge-centered cubic lattice.

The fragmentation threshold, f_F, is defined as the crack density at which opposite faces of the domain become separated; i.e., there is no contiguous cluster of Voronoi cells (Voronoi cells are contiguous if they share a face) connecting opposite faces of $\mathcal{D}$. Note that the crack density $f = 1 - f^*$, where f^* is the bond density on the dual of the Voronoi tessellation (face-centered lattice). Hence, the fragmentation threshold corresponds to the bond percolation threshold on the dual (f^*_{bond}) and $f_F = 1 - f^*_{\text{bond}}$. Although the fragmentation threshold is not a critical point for stiffness, it can be a critical point for phenomena that are reliant on the existence of percolating clusters, such as electrical or thermal conduction in materials with high interface resistance.

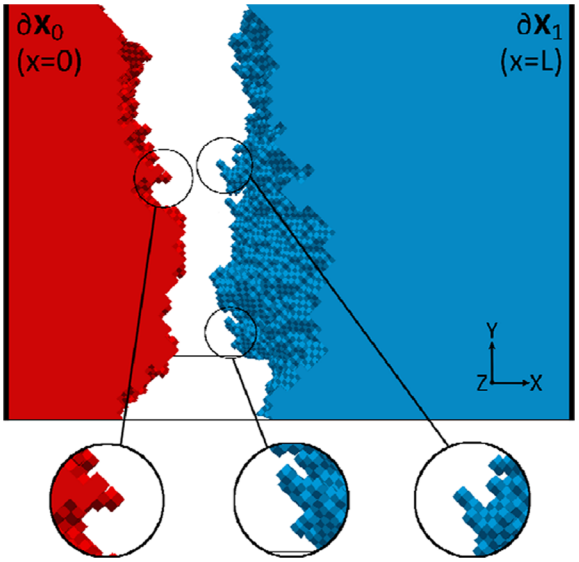

FIG. 1. Minimum-cut (minimum overhang) cleavage surface for a sample with $N = 30$ and $f = f_F = 0.88$. Red and blue indicate subdomains on the two sides of the minimum-cut surface, which are shifted horizontally for clarity. The cracks not comprising the minimum cut are not shown for clarity. The insets show details of a few overhangs.

The two geometric thresholds f_{c_T} and f_F can be evaluated using results from graph theory [28]. The transport percolation threshold, f_{c_T}, is not directly relevant to the present discussion, but is reported in order to outline the distinction with f_F. For the lattice used here, $f_{c_T} \cong 0.28$, which is close to the site percolation threshold for the body centered cubic lattice (which has the same coordination number of 8) of 0.246 [29,30]. The fragmentation threshold, f_F, is estimated based on the bond percolation threshold for the fcc dual lattice, $f^*_{\text{bond}} \cong 0.12$ [29], and hence $f_F = 1 - f^*_{\text{bond}} \cong 0.88$.

We evaluate the stiffness percolation threshold, f_{c_E}, in two steps. First, we define a geometric measure of interlocking in order to obtain a geometric approximation of the threshold, $f^g_{c_E}$. In the second step, we investigate the variation of the stiffness in the vicinity of the geometric estimate of f_{c_E}.

By definition, for $f \geq f_F$ there exists a nonempty set S of cleavage surfaces $S = \{CS_1, CS_2, \ldots\}$ separating opposite faces of the domain [say, the left face ∂X_0 ($x = 0$) and right face ∂X_1 ($x = L$) in Fig. 1], where a cleavage surface is defined as a contiguous (edge sharing) set of crack faces that span the cross section of the domain, i.e., yz plane in this case, and do not touch ∂X_0 or ∂X_1. An overhang parameter, m, can be defined for each such surface, based on the normalized projected area of the surface on the yz plane,

$$m^i = \frac{\sum_{j \in CS_i} |a_j \mathbf{n}_j . \mathbf{n}_1|}{L^2}, \tag{1}$$

where a_j and $\mathbf{n}_j$ are the area and unit normal of a crack face belonging to the cleavage surface CS_i, $\mathbf{n}_1$ is the unit normal oriented in the x-direction, and L^2 is the area of the cross

section of the model perpendicular to $\mathbf{n}_1$. If the cleavage surface has no overhangs, $m^i = 1$, while otherwise $m^i > 1$. Note that $m^i = 1$ does not imply that the cleavage surface is planar. The minimum of m^i over the population of cleavage surfaces S, $m = \min_i\{m^i\}$, represents the geometric measure of interlocking associated with the x-direction. If $m = 1$, there is no such interlocking and the structure can bear no tensile stress in the x-direction (see Fig. A2 in Supplemental Material [31]). To evaluate m, a graph is first created with nodes corresponding to the lattice points and bonds corresponding to the nearest-neighbor bonds. We now proceed to create a capacitated network [32] for our problem. All bonds are given an initial capacity of infinity. Further, based on the crack density fraction f, some bonds are randomly selected and given a capacity corresponding to their projected area (given by its dual Voronoi face) on the y-z plane, $|a_j\mathbf{n}_j.\mathbf{n}_1|$. Thus, if the total number of bonds (or Voronoi faces) is N_B, then fN_B are cracked and have capacities corresponding to their projected areas, while $(1\text{-}f)N_B$ bonds have infinite capacities. A source node is attached to the graph with additional bonds connecting it to all the nodes (lattice points) lying on the left face of the domain, ∂X_0, while a sink node is similarly attached with additional bonds connecting it to the right face of the domain, ∂X_1. These source or sink bonds have infinite capacities. Next, the max flow in the graph from source to sink is computed by the Boykov-Kolmogorov algorithm [33] provided as a part of the BOOST library [34]. By the max-flow min-cut theorem [28], this also identifies the minimum cut that separates the source and the sink. As a consequence of the way the weights are defined, the max flow is equal to mL^2 [35] and the min cut corresponds to the cleavage surface with minimum interlocking. Further details are provided in Supplemental Material [31]. As indicated above, the variation of the replica-averaged m, $\bar{m}$, with f provides a geometric estimate of the stiffness percolation threshold, f_{c_E}. This problem bears close resemblance to first passage percolation in 2D [36], which has been generalized to higher dimensions [37,38].

The variation of the interlocking parameter, $\bar{m} - 1$, with crack density f is shown in Fig. 2. Models of three different sizes are considered, with $N = 50$, 70, and 100. $(\bar{m} - 1)$ is nonzero for $f_F < f \leq 0.95$ but decreases rapidly to 0 at the upper end of this interval. This indicates the presence of overhangs that lead to interlocking. The variation of $(\bar{m} - 1)$ in the vicinity of the point where this quantity vanishes is shown in log-log coordinates in the inset to Fig. 2. For the largest system considered, with $N = 100$, we observe that $\bar{m} - 1 \sim (f^g_{c_E} - f)^\gamma$, where the geometric estimate of f_{c_E}, $f^g_{c_E}$, and the exponent γ are treated as free parameters. The inferred values $f^g_{c_E} = 0.945 \pm 0.001$ and $\gamma = 2.90 \pm 0.24$ lead to the power function shown in the figure. This represents an upper bound for f_{c_E}, as the structure cannot provide resistance to tensile loads if the minimum cut surface has no interlocking.

The stiffness of the microcracked continuum is estimated by modeling it as an elastic spring network on the underlying

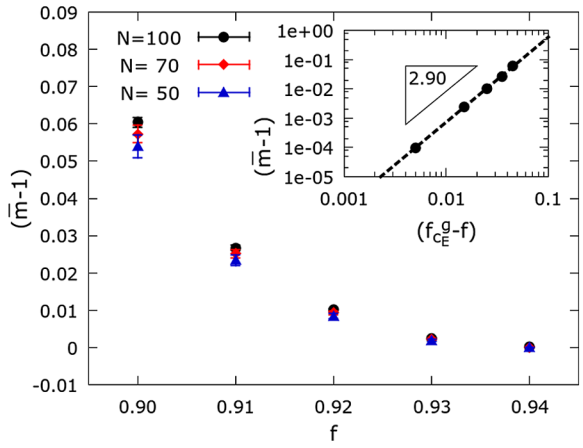

FIG. 2. Average interlocking parameter $\bar{m} - 1$ for the minimum-cut surface as a function of crack density f and for several model sizes, N. The model size does not affect significantly $\bar{m}$ close to the critical point where $\bar{m} - 1 = 0$. For $f \leq f_F \cong 0.88$ no cleavage surface exists, and $\bar{m}$ is not defined. For $f_F < f < 1$ at least one cleavage surface exists that may exhibit interlocking. The inset shows a power law fit to the data with exponent $\gamma = 2.90$ and $f^g_{c_E} = 0.945$, which is a geometric estimate of the stiffness percolation threshold f_{c_E}.

fcc lattice. Harmonic potentials are used to model nearest-neighbor bonds and nearest-neighbor angles such that the model corresponds to a material with cubic anisotropy. Interactions across cracked surfaces are modeled with the bonds replaced by purely repulsive Lennard-Jones interactions with cutoff equal to the nearest-neighbor distance in the underlying fcc lattice. These model cracks of zero thickness in the unloaded state. One face of the cubic domain is held fixed, while the opposite face is displaced. Traction-free boundary conditions are applied on all other model faces. Since at large values of f fragments from the free surfaces may detach, we prevent this outward rigid body mode by confining dilatation in the directions perpendicular to the tensile loading direction. The values of all material parameters used are provided in Supplemental Material [31].

The variation of the stiffness of the microcracked continuum with f is shown in Fig. 3 for the entire range of f, from 0 to 1, and for models with $N = 30$. At low crack densities, when $f \to 0$, the effective modulus is weakly dependent on the crack density. Various estimates are available in the literature for this range [12]. The continuous line corresponds to a model with randomly oriented noninteracting cracks that predicts $E_{\text{eff}}/E_0 = 1/(1 + \beta f)$, where E_{eff} is the effective stiffness of the structure measured in uniaxial tension. The values of β and E_0 are discussed in Supplemental Material [31]. Alternative approaches to handling crack-crack interaction and nonlinearities introduced by crack closure have been developed in the damage mechanics literature [39].

For $f > f_F$, the structure is loaded primarily via the contacts at the interlocked surfaces, but the overall strain energy is still a quadratic function at small strains and hence

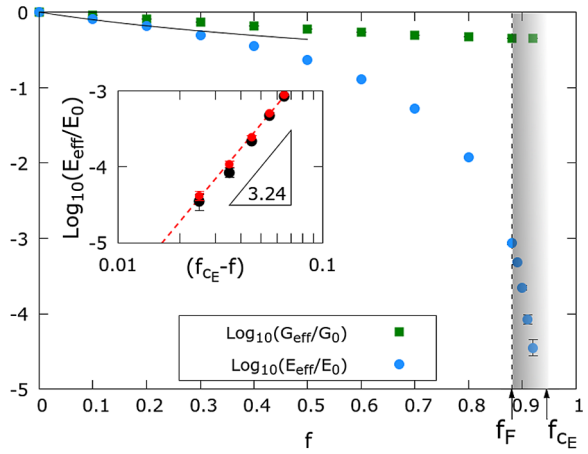

FIG. 3. Variation of the effective tensile Young's modulus E_{eff} (blue circles) and shear modulus G_{eff} (green squares) of the structure, normalized by the corresponding moduli of the uncracked material, versus the crack density (f) for a model with $N = 30$. At low densities ($f < 0.3$), the variation for E_{eff} is represented well by $E_{\text{eff}}/E_0 = 1/(1 + \beta f)$, with $\beta = 2.6$ [12]. At $f = f_F = 0.88$ the crack density is high enough for fragmentation to occur; beyond this point the structure is loaded via topological interlocking of the irregularly shaped fragments. At $f = f_{c_E} = 0.945 \pm 0.005$ Young's modulus vanishes (stiffness percolation threshold). The inset shows the variation of E_{eff} with the distance to f_{c_E} for systems with $N = 30$ (black) and $N = 50$ (red). The shear modulus does not exhibit critical behavior. The range of crack densities marked in gray in the main figure represents the state in which the material is fully fragmented but preserves stiffness due to topological interlocking.

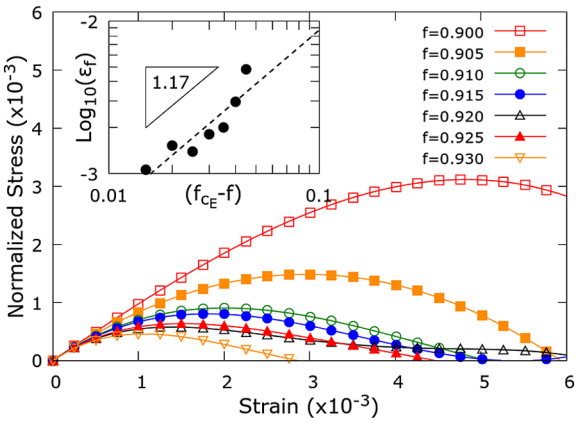

FIG. 4. Stress-strain curves for systems with various f values in the regime of interlocking. The vertical axis is normalized by the effective modulus, E_{eff}, reported in Fig. 3. The inset shows the scaling of the strain at peak stress near f_{c_E}.

E_{eff} is well defined in this limit. We identify the stiffness percolation threshold by fitting a power law of the form $(E_{\text{eff}}/E_0) = (fc_E - f)^{\alpha}$ to the blue circles in Fig. 3 (black symbols in the inset to Fig. 3). The fit leads to $fc_E = 0.945 \pm 0.005$ and $\alpha = 3.24 \pm 0.42$. Although this threshold is similar to the geometric estimate, the scaling exponent is different from the geometric exponent γ. This is not surprising as the geometric overhang is a measure of only the minimum-cut surface, while the stiffness is a global measure that depends on all loaded interfaces in the structure. For $f > f_{C_E}$, the cleavage surfaces have no overhangs and the structure has no stiffness.

The important result here is the existence of a range of crack densities, $f_F < f < f_{C_E}$ (shown in gray in Fig. 3), in which the structure, although fragmented, exhibits at small strains a quadratic strain energy function and well-defined (but different) elastic moduli in both tension and compression. Such samples are neither continua nor jammed granular packings.

The shear modulus was evaluated for all systems shown in Fig. 3 by applying a simple shear loading to the model. Interestingly, the shear modulus is finite at f_{c_E} and the value at the threshold is only 56% smaller than the bulk shear modulus of the uncracked material, G_0. This is expected as the fully cracked state ($f = 1$) corresponds to a close packed and ordered frictionless granular system of rhombic dodecahedra. The Young's modulus measured in compression is identical to the modulus of the uncracked material. Hence, the system exhibits behavior compatible with both the first and second order phase transitions, similar (but not identical) to the jamming transition [8–10].

To demonstrate the evolution of the material behavior as f increases in the interlocking regime, $f_F < f < f_{c_E}$, Fig. 4 shows the stress-strain curves evaluated for several models. The stress is normalized by E_{eff} reported in Fig. 3 such that all curves have slope 1 at small strains. At the fragmentation limit $f = f_F = 0.88$ (and below), the behavior is linear elastic, as expected. As f increases, interlocking of fragments provides stiffness at small strains, but disengagement occurs at larger strains leading to a peak in the stress-strain curve. The peak shifts to smaller strains and stresses as f increases. The curve converges to the horizontal axis at $f = f_{c_E}$ (Fig. 3). The strain at peak stress exhibits also a power law scaling for values of f near f_{c_E}, $\varepsilon_f \sim (fc_E - f)^{\alpha_\varepsilon}$, with $\alpha_\varepsilon = 1.17$ (see inset to Fig. 4).

The size effect was studied by using models of different sizes, with N ranging from 30 to 100 for the geometric estimate $f^g_{c_E}$, and from 30 to 50 for the mechanical estimate, f_{c_E}. Both parameters are weakly sensitive to the model size. The size effect on $f^g_{c_E}$ is shown in Fig. 2 and the inset to Fig. 3.

In this study, we demonstrate the existence of a fully fragmented material state resulting from increasing density of microcracks in which the material preserves stiffness due to the interlocking of fragments. The stress-strain curve in this range is nonlinear, despite the fact that the bulk material behavior is linear elastic. The analysis provides the range of crack densities in which this behavior is expected, which can be used to guide experiments aimed at producing stochastically interlocked materials. Such materials preserve stiffness and are resilient relative to additional damage produced by localized loading or thermal shock.

*Corresponding author.
picuc@rpi.edu

[1] M. F. Thorpe, Continuous deformations in random networks, J. Non-Cryst. Solids **57**, 355 (1983).
[2] D. J. Jacobs and M. F. Thorpe, Generic Rigidity Percolation: The Pebble Game, Phys. Rev. Lett. **75**, 4051 (1995).
[3] M. Latva-Kokko and J. Timonen, Rigidity of random networks of stiff fibers in the low-density limit, Phys. Rev. E **64**, 066117 (2001).
[4] A. J. Liu and S. R. Nagel, Nonlinear dynamics: Jamming is not just cool any more, Nature (London) **396**, 21 (1998).
[5] M. van Hecke, Jamming of soft particles: Geometry, mechanics, scaling and isostaticity, J. Phys. Condens. Matter **22**, 033101 (2010).
[6] S. Feng and P. N. Sen, Percolation on Elastic Networks: New Exponent and Threshold, Phys. Rev. Lett. **52**, 216 (1984).
[7] W. G. Ellenbroek, Z. Zeravcic, W. van Saarloos, and M. van Hecke, Nonaffine response: Jammed packings vs spring networks, Europhys. Lett. **87**, 34004 (2009).
[8] D. A. Head, Critical Scaling and Aging in Cooling Systems Near the Jamming Transition, Phys. Rev. Lett. **102**, 138001 (2009).
[9] C. P. Goodrich, S. Dagois-Bohy, B. P. Tighe, M. van Hecke, A. J. Liu, and S. R. Nagel, Jamming in finite systems: Stability, anisotropy, fluctuations, and scaling, Phys. Rev. E **90**, 022138 (2014).
[10] W. G. Ellenbroek, V. F. Hagh, A. Kumar, M. F. Thorpe, and M. van Hecke, Rigidity Loss in Disordered Systems: Three Scenarios, Phys. Rev. Lett. **114**, 135501 (2015).
[11] J. Wilhelm and E. Frey, Elasticity of Stiff Polymer Networks, Phys. Rev. Lett. **91**, 108103 (2003).
[12] M. Kachanov, Elastic solids with many cracks and related problems, Adv. Appl. Mech. **30**, 259 (1993).
[13] D. Krajcinovic, Effective material properties in the limit of large defect concentration, Eng. Fract. Mech. **57**, 227 (1997).
[14] R. C. Picu, A. Pal, and M. V. Lupulescu, Interlocking-induced stiffness in stochastically microcracked materials beyond the transport percolation threshold, Phys. Rev. E **93**, 043005 (2016).
[15] M. Wyart, H. Liang, A. Kabla, and L. Mahadevan, Elasticity of Floppy and Stiff Random Networks, Phys. Rev. Lett. **101**, 215501 (2008).
[16] J.-H. Lee, J. P. Singer, and E. L. Thomas, Micro/nanostructured mechanical metamaterials, Adv. Mater. **24**, 4782 (2012).
[17] A. A. Zadpoor, Mechanical metamaterials, Materials Horizons **3**, 371 (2016).
[18] A. V. Dyskin, Y. Estrin, A. J. Kanel-Belov, and E. Pasternak, A new concept in design of materials and structures: assemblies of interlocked tetrahedron-shaped elements, Scr. Mater. **44**, 2689 (2001).
[19] Y. Estrin, A. V. Dyskin, and E. Pasternak, Topological interlocking as a material design concept, Mater. Sci. Eng. C **31**, 1189 (2011).
[20] J. D. Hiller, J. Miller, and H. Lipson, Microbricks for three-dimensional reconfigurable modular microsystems, J. Microelectromech. Syst. **20**, 1089 (2011).
[21] S. Khandelwal, T. Siegmund, R. J. Cipra, and J. S. Bolton, Scaling of the elastic behavior of two-dimensional topologically interlocked materials under transverse loading, J. Appl. Mech. **81**, 031011 (2013).
[22] A. v. Dyskin, Y. Estrin, E. Pasternak, H. c. Khor, and A. j. Kanel-Belov, Fracture resistant structures based on topological interlocking with nonplanar contacts, Adv. Eng. Mater. **5**, 116 (2003).
[23] Y. Feng, T. Siegmund, E. Habtour, and J. Riddick, Impact mechanics of topologically interlocked material assemblies, Int. J. Impact Eng. **75**, 140 (2015).
[24] K. Miszta *et al.*, Hierarchical self-assembly of suspended branched colloidal nanocrystals into superlattice structures, Nat. Mater. **10**, 872 (2011).
[25] S. Suresh, C. F. Shih, A. Morrone, and N. P. O'Dowd, Mixed-mode fracture toughness of ceramic materials, J. Am. Ceram. Soc. **73**, 1257 (1990).
[26] M. B. Dusseault, Itacolumites: The flexible sandstones, Quarterly J. Eng. Geology Hydrogeology **13**, 119 (1980).
[27] T. Shimazu, M. Miura, N. Isu, T. Ogawa, K. Ota, H. Maeda, and E. H. Ishida, Plastic deformation of ductile ceramics in the Al_2TiO_5–$MgTi_2O_5$ system, Mater. Sci. Eng. A **487**, 340 (2008).
[28] C. Papadimitriou and K. Steiglitz, *Combinatorial Optimization: Algorithms and Complexity* (Dover Publications, New York, 1982).
[29] C. D. Lorenz and R. M. Ziff, Precise determination of the bond percolation thresholds and finite-size scaling corrections for the sc, fcc, and bcc lattices, Phys. Rev. E **57**, 230 (1998).
[30] C. D. Lorenz and R. M. Ziff, Universality of the excess number of clusters and the crossing probability function in three-dimensional percolation, J. Phys. A **31**, 8147 (1998).
[31] See Supplemental Material at http://link.aps.org/supplemental/10.1103/PhysRevLett.119.085502 for description of the geometric model, elastic model, and scaling of stiffness at small crack densities.
[32] L. R. Ford, Jr. and D. R. Fulkerson, *Flows in Networks* (Princeton University Press, Princeton, 2010).
[33] Y. Boykov and V. Kolmogorov, An experimental comparison of min-cut/max- flow algorithms for energy minimization in vision, IEEE Trans. Pattern Analysis Machine Intelligence **26**, 1124 (2004).
[34] J. G. Siek, L.-Q. Lee, and A. Lumsdaine, *Boost Graph Library, The User Guide and Reference Manual*, 1st ed. (Addison-Wesley Professional, New York, 2001).
[35] G. R. Grimmett, in *Percolation* (Springer, New York, 1999), pp. 378–380.
[36] G. Grimmett and H. Kesten, First-passage percolation, network flows, and electrical resistances, Z. Wahrsch. Verw. Geb. **66**, 335 (1984).
[37] H. Kesten, Percolation theory and first-passage percolation, Ann. Probab. **15**, 1231 (1987).
[38] M. Aizenman, J. T. Chayes, L. Chayes, J. Fröhlich, and L. Russo, On a sharp transition from area law to perimeter law in a system of random surfaces, Commun. Math. Phys. **92**, 19 (1983).
[39] G. Z. Voyiadjis and P. I. Kattan, *Damage Mechanics* (CRC Press, Taylor and Francis Group, Boca Raton, FL, 2005).